The JWST FRESCO Survey: Legacy NIRCam/Grism Spectroscopy and Imaging in the two GOODS Fields

P. A. Oesch[1,2]★, G. Brammer[2], R. P. Naidu[3]†, R. J. Bouwens[4], J. Chisholm[5], G. D. Illingworth[6], J. Matthee[7], E. Nelson[8], Y. Qin[9,10], N. Reddy[11], A. Shapley[12], I. Shivaei[13], P. van Dokkum[14], A. Weibel[1], K. Whitaker[15,2], S. Wuyts[16], A. Covelo-Paz[1], R. Endsley[5], Y. Fudamoto[17,18], E. Giovinazzo[1], T. Herard-Demanche[4], J. Kerutt[19], I. Kramarenko[1], I. Labbe[20], E. Leonova[21,22], J. Lin[23], D. Magee[6], D. Marchesini[23], M. Maseda[24], C. Mason[2], J. Matharu[2], R. A. Meyer[25,1], C. Neufeld[14], G. Prieto Lyon[2], D. Schaerer[1], R. Sharma[16], M. Shuntov[2], R. Smit[26], M. Stefanon[27,28], J. S. B. Wyithe[9,10], M. Xiao[1]

Affiliations are listed at the end of the paper

ABSTRACT

We present the JWST Cycle 1 53.8hr medium program FRESCO, short for "First Reionization Epoch Spectroscopically Complete Observations". FRESCO covers 62 arcmin^2 in each of the two GOODS/CANDELS fields for a total area of 124 arcmin^2 exploiting JWST's powerful new grism spectroscopic capabilities at near-infrared wavelengths. By obtaining ~2hr deep NIRCam/grism observations with the F444W filter, FRESCO yields unprecedented spectra at R ~ 1600 covering 3.8 to 5.0 μm for most galaxies in the NIRCam field-of-view. This setup enables emission line measurements over most of cosmic history, from strong PAH lines at $z \sim 0.2 - 0.5$, to Paα and Paβ at $z \sim 1 - 3$, HeI and [SIII] at $z \sim 2.5 - 4.5$, Hα and [NII] at $z \sim 5 - 6.5$, up to [OIII] and Hβ for z~7-9 galaxies. FRESCO's grism observations provide total line fluxes for accurately estimating galaxy stellar masses and calibrating slit-loss corrections of NIRSpec/MSA spectra in the same field. Additionally, FRESCO results in a mosaic of F182M, F210M, and F444W imaging in the same fields to a depth of ~ 28.2 mag (5 σ in 0.″32 diameter apertures). Here, we describe the overall survey design and the key science goals that can be addressed with FRESCO. We also highlight several, early science results, including: spectroscopic redshifts of Lyman break galaxies that were identified almost 20 years ago, the discovery of broad-line active galactic nuclei at $z > 4$, and resolved Paα maps of galaxies at $z \sim 1.4$. These results demonstrate the enormous power for serendipitous discovery of NIRCam/grism observations.

Key words: surveys – dark ages, reionization, first stars – galaxies: formation – galaxies: evolution – galaxies: high-redshift

1 INTRODUCTION

Revealing the dramatic build-up of galaxies from $z > 6$ to the peak of star formation at z~2-3 is one of astronomy's great achievements with the Hubble and Spitzer Space Telescopes. Data from these observatories revealed that the first 1 Gyr of cosmic history ($z > 6$) was a time of rapid change: soon after the birth of the first stars from metal-free primordial gas, the galaxy population grew rapidly both in star-formation and stellar mass (e.g., Finkelstein 2016; Stark 2016; Oesch et al. 2018; Bouwens et al. 2023). After $z \sim 8$, the star-formation and stellar mass density grew ~10-30× up to the peak of cosmic star formation at $z \sim 2 - 4$ (see Fig 7; e.g., Madau & Dickinson 2014; Bouwens et al. 2015a; Song et al. 2016; Davidzon et al. 2017; Furtak et al. 2021; Stefanon et al. 2021).

Even though this general picture of early galaxy build-up is well established, the foundation it stands on remains uncertain. In particular, HST-based analyses only probe the rest-frame ultra-violet

(UV) of $z > 3$ galaxies, which can lead to a bias against dusty or old galaxies (e.g., Casey et al. 2014, 2018; Wang et al. 2019; Xiao et al. 2023; Barrufet et al. 2023; Rodighiero et al. 2023). Additionally, broad-band rest-frame optical imaging can be contaminated by extremely strong emission lines that appear to be common at $z \geq 4$, complicating accurate measurements of the underlying continuum and inferences of stellar masses and ages (e.g., Schaerer & de Barros 2009; Labbé et al. 2013; Stark et al. 2013; Bisigello et al. 2019; Endsley et al. 2023; Stefanon et al. 2022).

The most significant shortcoming before the advent of JWST, however, remained the lack of spectroscopically confirmed redshifts. In particular, studies exploring the earliest galaxies in the Epoch of Reionization (EoR) with spectroscopy were sparse before JWST due to disappearing Lyα lines in the neutral IGM (e.g., Stark et al. 2010; Treu et al. 2013; Pentericci et al. 2014), and due to low Lyα fractions in general. Consequently, at $z > 7$, only a handful of luminous galaxies had spectroscopic confirmations, based on Lyα or weak rest-frame UV emission (e.g., Oesch et al. 2015; Stark et al. 2017), or from ALMA ISM lines (e.g., Inoue et al. 2016; Hashimoto et al. 2018; Bakx et al. 2020; Schouws et al. 2022; Bouwens et al. 2022).
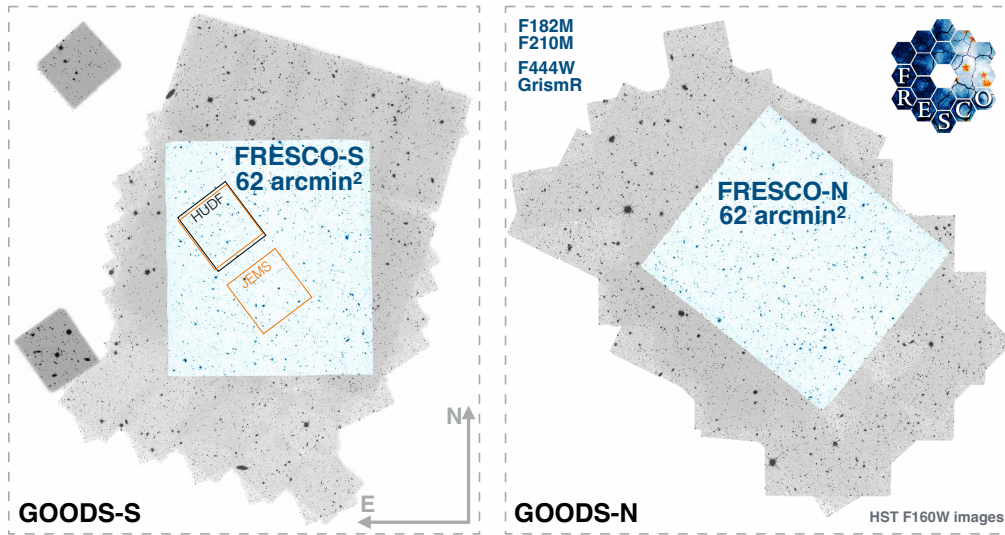
★ E-mail: pascal.oesch@unige.ch
† Hubble Fellow

Figure 1. FRESCO was designed to cover the majority of the two CANDELS/Deep regions in the GOODS-S and -N fields, which are among the most valuable extragalactic legacy fields in the full sky. Among others, the FRESCO fields overlap with the medium-band survey JEMS (orange) that covers the original HUDF/XDF (black). The vast amount of ancillary data available in these fields made these fields the obvious choice for spectroscopic follow-up. At the highest redshifts, more than 40% of all known $z \sim 7 - 8$ candidate galaxies lie in these fields, with GOODS-N featuring an overdensity of $z \sim 7 - 8$ candidates. Additional overdensities are known to exist at lower redshifts, which will be mapped out with these data. The FRESCO mosaics are obtained in a 4×2 mosaic with partial overlap for optimal wavelength coverage. The total area amounts to 7.3×8.5 arcmin^2 both with grism spectroscopy and medium band imaging, which further enhances the legacy value of these fields.

This caused extra uncertainty given that the inferences on galaxy abundances at high redshift are statistical in nature. The agreement between candidate catalogs from different teams often remained limited, even when based on the same data: <60% overall, dropping to $\sim 30\%$ at the faint end (e.g., compare catalogs from Bouwens et al. 2015a; Finkelstein et al. 2015). Similarly, blind spectroscopic surveys, e.g., with VIMOS or MUSE, up to $z \sim 6$ consistently showed that a non-negligible fraction (up to 60%) of genuine high-redshift galaxies can be missed in traditional Lyman Break color-color selections due to scatter in their observed colors (e.g., Le Fèvre et al. 2015; Inami et al. 2017).

With the advent of multiplexed infrared spectroscopy of the James Webb Space Telescope (JWST), all these issues that plagued the exploration of early galaxies can finally be overcome. Already after just a few months of observations with JWST, extremely early galaxy candidates are now identified out to $z \sim 12 - 16$ (e.g., Bouwens et al. 2023; Harikane et al. 2022; Donnan et al. 2023; Naidu et al. 2022; Finkelstein et al. 2022; Atek et al. 2023; Adams et al. 2023) and spectroscopically confirmed to $z \sim 13$ (e.g., Curtis-Lake et al. 2022; Bunker et al. 2023; Arrabal Haro et al. 2023). Additionally, rest-frame optical photometry and galaxy selections are enabled beyond $z > 3$ (e.g., Barrufet et al. 2023; Rodighiero et al. 2023; Nelson et al. 2023; Pérez-González et al. 2023).

In this paper, we present the JWST FRESCO survey, short for "First Reionization Epoch Spectroscopically Complete Observations" (GO-1895; PI Oesch). FRESCO fully exploits the unprecedented grism spectroscopic ability of *JWST* at $\sim 4 - 5 \, \mu$m to obtain a *complete* sample of early star-forming emission line galaxies down to $\sim 2 \times 10^{-18}$erg s^{-1} cm^{-2} across cosmic history in two ~62 arcmin^2 F444W NIRCam/grism mosaics in the extragalactic legacy fields CANDELS/Deep in GOODS-South and North (Figure 1).

FRESCO is designed to obtain a spectrum with $R \sim 1600$ for every reionization-era galaxy in the field down to ~0.2-0.5 L_{*UV}, probing the strong rest-frame optical emission lines [OIII]+Hβ at $z = 6.7 - 9.0$

Field	RA	DEC	Area [arcmin^2]
FRESCO-S	03:32:31	−27:48:04	60.9 (grism)
			62.4 (imaging)
FRESCO-N	12:36:46	+62:14:45	60.9 (grism)
			62.4 (imaging)

Table 1. Summary of the FRESCO fields and areas.

and Hα+[NII] at $z = 4.9 - 6.6$, in addition to other emission lines across the full cosmic history. This includes dust-insensitive Paschen lines at $z \sim 1 - 3$, as well as PAH 3.3 μm lines at $z < 0.5$. Therefore, the FRESCO observations enable accurate measurements of early star formation and stellar mass build up; provide detailed insights into early, low-metallicity star formation; reveal small scale 3D clustering and measure the contribution of mergers to early galaxy assembly. These key science cases will be discussed in this paper, after first introducing the survey design.

This paper is organized as follows: in Section 2, we introduce the observational design of the FRESCO grism and imaging survey. In Section 3, we describe the main scientific goals of FRESCO, before we end with a summary in Section 4. Throughout this paper a standard ΛCDM cosmology is adopted with H$_0$ = 70 km s^{-1}Mpc^{-1}, Ω_M = 0.3, and Ω_Λ = 0.7.

2 OBSERVATIONAL DESIGN

The primary goals of FRESCO are to resolve two of the key limitations of our current understanding of the galaxy stellar mass build-up during the epoch of reionization at $z > 6$: (1) uncertain redshifts and outlier fractions, and (2) unknown emission line contribution to rest-frame optical broad-band photometry. In the following, we outline the survey design to overcome these limitations.
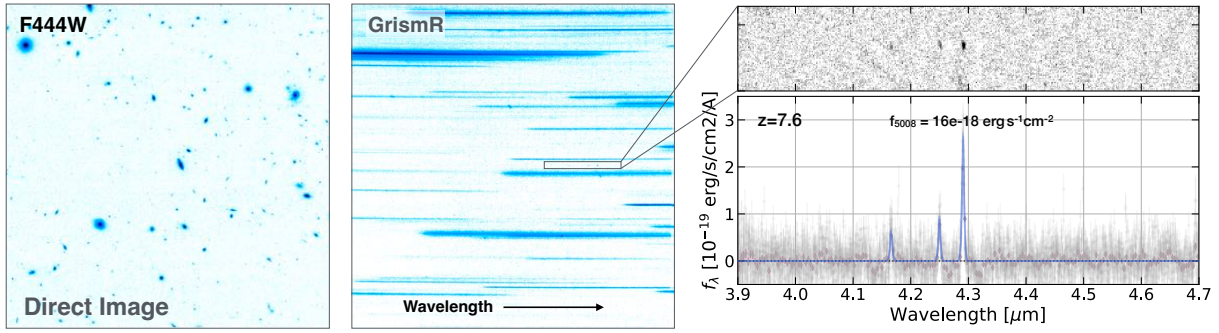
Figure 2. Example of FRESCO's spectroscopic strategy. The left panel shows a portion of the F444W direct image in the FRESCO-S field. The middle panel shows the associated GrismR data, from which FRESCO can identify EoR galaxies as emission line sources. Down to UV continuum magnitudes of 26.8, $z = 6.7 - 9.0$ sources are expected to show three emission lines from the [OIII] doublet as well as Hβ, resulting in unambiguous redshift identifications. For example, the right panels show the 2D and the extracted 1D spectra of a source in the FRESCO-S field with an unambiguous grism redshift at $z = 7.6$.

2.1 Slitless Grism Spectra

The core of FRESCO is NIRCam slitless grism observations, which result in a spectrum for every source in the field-of-view (see, e.g., Sun et al. 2022). FRESCO follows in the footsteps of numerous successful grism surveys conducted with HST such as 3D-HST (Brammer et al. 2012; Momcheva et al. 2016), GLASS (Treu et al. 2015), FIGS (Pirzkal et al. 2018), CLEAR (Estrada-Carpenter et al. 2019), WISP (Atek et al. 2010), and GRAPES (Pirzkal et al. 2004), but with greater sensitivity, at longer wavelength, and with spectral resolution a factor 10× higher.

Unlike traditional slit-based spectroscopy that can only target preselected sources, slitless spectra effectively provide a complete sample of emission line selected galaxies. With JWST, the NIRISS instrument provides slitless spectra up to ~2μm. The NIRCam camera (Rieke et al. 2005, 2023) includes a grism mode at longer wavelengths, providing spectra at relatively high resolution, R~1600, up to 5μm. In cycle 1, this mode is only used by a few programs, including the GTO/EIGER survey (Kashino et al. 2023; Matthee et al. 2023b), as well as the ERS/CEERS program (Finkelstein et al. 2022), who are all using the F356W filter. As we will show below, such grism observations at 3-5 μm are extremely powerful probes of galaxy build-up across cosmic history.

2.1.1 Choice of Filter and Grism

Grism observations can use the same set of medium and wide filters as NIRCam imaging in its long-wavelength (LW) channel. The choice of filter determines the wavelength range of the spectra. The key redshift range that FRESCO targets is $z > 6$, i.e., the reionization epoch, where spectroscopic redshifts can be determined from strong rest-optical emission lines such as Hα+[NII] and [OIII]+Hβ. FRESCO therefore obtains 4-5μm grism spectra with the F444W filter. This setup allows us to probe Hα+[NII] lines for galaxies at $z = 4.9 - 6.6$ and [OIII]+Hβ lines from $z = 6.7 - 9.0$. If bright enough, the [OII] line could in principle even be detected in sources at $z = 9.3 - 12.5$. Hence, the F444W grism spectra result in near complete coverage of the epoch of reionization out to some of the most distant galaxies known in the Universe.

NIRCam is equipped with two different grisms in the LW channel that provide the same spectral resolution, but have a dispersion direction that is rotated by 90 degree relative to each other (GrismR and GrismC). FRESCO is using only one of them: GrismR. The advantages of taking data with both grisms are a better handle on contami-

nation along the dispersion direction and unambiguous identification of sources in the direct image from which the spectra originate. Unfortunately, using GrismC results in a disproportionate increase of overheads, given that out-of-field images need to be taken at 35″ offsets, which results in separate visits. As an example, if both GrismC and GrismR were used, FRESCO's survey time would have increased by 15hrs (~30%) without any gain in sensitivity. Even with only one grism observation, most shortcomings can be mitigated, as demonstrated by the extremely successful HST grism survey 3D-HST, from which the community has built extensive experience to deal with overlapping spectra (Brammer et al. 2012). Due to these excessive overhead costs, FRESCO is obtained with GrismR observations only, similarly to the GTO/EIGER survey (GTO-1243; PI Lilly).

2.1.2 NIRCam/Grism Mosaic and Wavelength Coverage

The wavelength coverage of the NIRCam/grism depends on the location of the source on the detector. At a wavelengths of 3.95 μm, the F444W grism and the direct image coincide. However, at other wavelengths, the positions are shifted by 9.85Å/pixel, varying only slightly across the field. This means that only a certain fraction of sources from the direct image will obtain complete spectral coverage. Additionally, the grism spectra cover sources from outside the field-of-view. The GrismR spectra of detector A and B are dispersed in the opposite direction. By obtaining a second pointing offset by ~ 1.8 arcmin, FRESCO achieves coverage over 3.9-4.4 μm over almost the full field of view and partial coverage from 3.9-5 μm over 4.9 arcmin in x-direction. In the y-direction, FRESCO obtained 4 pointings with minimal overlap (thus spanning 8.5 arcmin). Therefore, each FRESCO field covers 6.7×8.5 arcmin² (57 arcmin²) at 3.9-4.4 μm and 4.9×8.5 arcmin² (42 arcmin²) at 3.9-5 μm (corresponding to 73% of the full mosaic shown in Figure 1). More details on the spectral coverage and the spectral extraction will be provided in Brammer et al., in prep.

2.1.3 Exposure Times and Sensitivity

FRESCO is designed to reach a 5σ emission-line sensitivity for NIRCam/grism observations of ~2×10^{-18} erg s^{-1} cm^{-2} (for compact sources), which is the expected [OIII]5008 flux of sources at 1 mag below L$_\star$ at $z = 7 - 9$ (based on the LF derived from De Barros et al. 2019; see also Matthee et al. 2023b). This is achieved with eight grism exposures of 880s taken with the MEDIUM2 readout mode with 9 groups for each pointing. This results in a total grism

Filter	Exposures	Time [s]	5σ Depth
F444W grism	8	7043	2×10^{-18} erg s^{-1} cm^{-2}
F444W imaging	3	934	28.2 mag
F210M imaging	8	3522	28.2 mag
F182M imaging	11	4456	28.4 mag

Table 2. Summary of exposure times per FRESCO pointing. In total, 2 mosaics of 4×2 pointings were obtained. Line sensitivity estimated for compact sources, integrated over full extension of the line. Imaging depths measured as the 5σ rms in 0″32 diameter apertures, without corrections to total fluxes.

exposure time of 7043 s at each position (see also Table 2). Four large scale dithers are used, but no sub-pixel dithering. The grism exposures are taken in two sets of these four-point dithers, in each set using a different short-wavelength filter for imaging (see Sect. 2.2). An example of the resulting FRESCO imaging and spectroscopy in the GOODS-S field is shown in Figure 2.

2.1.4 Grism Data Reduction

Details of the NIRCam/grism data reduction will be provided in a data release paper (Brammer et al, in prep). Briefly, we use the publicly available `grizli` code[1], with slightly modified sensitivity curves and spectral traces based on the v4 grism configuration files provided by Nor Pirzkal[2]. `grizli` is used to reduce all images and spectra and to align them to Gaia-matched reference frames. Given that we are mostly interested in emission line detections, continuum subtracted spectra are created using a running median filter along each row. Following Kashino et al. (2023), the filter uses a 12 pixel central gap to minimize self-subtraction. For each source in the imaging catalog, optimally extracted spectra are then produced based on the individual input exposures. The spectral catalogs will be released together with individual science papers and with a future data release paper.

2.2 FRESCO's Imaging Legacy

Simultaneous with the grism spectra, FRESCO obtains NIRCam medium band images in two short-wavelength filters (F182M and F210M) to extend the space-based legacy data in these fields to 1.8 and 2.1 μm down to 28.3 mag (at 5σ). These medium-band filters seamlessly extend the NIR wavelength coverage of the HST data in the CANDELS/Deep area, complementing the GTO/JADES NIRCam imaging. These data improve the UV spectral slope measurement of $z > 7$ galaxies and, at lower redshift, allow the community to push rest-frame optical imaging analyses beyond the peak of cosmic star formation, from $z \sim 2.5$ to beyond $z \sim 4$.

After the grism exposures, three direct and out-of-field images are taken in the F444W filter. These images are needed to associate the spectra with individual galaxies. The exposure times of these direct images are set to produce a $> 4\sigma$ detection of every single galaxy for which a significant emission-line detection is expected. This ensures that spectra can be associated with the imaged galaxies in the field. FRESCO thus obtained 934s exposures in F444W, split over three offset positions, leading to a 5σ-depth of 28.2 mag (see Table 2).

The medium-band images are taken with the same readout mode as the grism exposures (MEDIUM2, 9 groups), resulting in an exposure
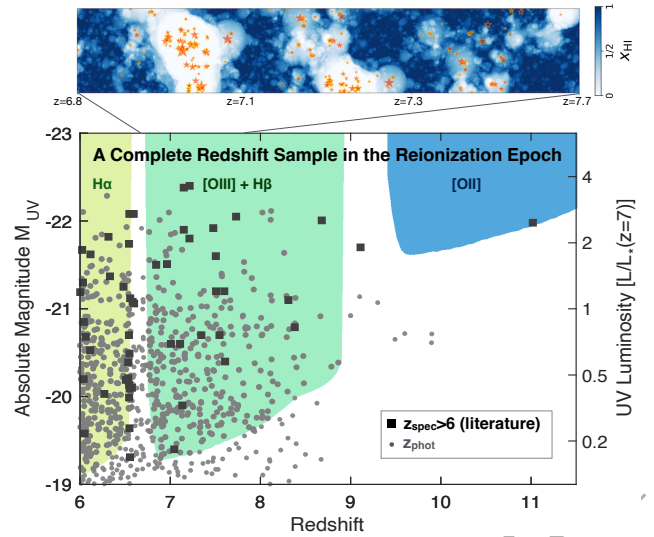

Figure 3. The average spectroscopic sensitivity of the FRESCO survey to observe strong rest-frame optical emission lines during the epoch of reionization. Before the advent of JWST, less than 1% of known sources at $z > 6$ had spectroscopically confirmed redshifts. FRESCO is obtaining complete samples with spec-z down to $M_{UV} = -19$ ($z \sim 6$) to -20 ($z \sim 8$) thanks to strong Hα and [OIII]+Hβ lines, respectively. This allows us to map out the large-scale structure during cosmic reionization. Simulations predict that ionized regions first appear around overdensities as shown by a slice through the DRAGONS simulation (top panel). The 3D large scale structure during the epoch of reionization will for the first time be revealed thanks to FRESCO redshifts.

time of 3522s each. The F182M filter is used during the three F444W imaging exposures, which are taken with the SHALLOW4 readout pattern with 6 groups. It thus receives an additional integration of 934s. The total exposure times per pointing for each filter are listed in Table 2.

2.3 Target Fields

FRESCO is split into two separate fields with an equal setup covering two of the most well-studied fields in the sky: the central regions of the two GOODS fields (North and South; Giavalisco et al. 1996). These were also covered by the Deep tier of the CANDELS survey (Koekemoer et al. 2011; Grogin et al. 2011). In GOODS-South, the FRESCO field further covers the HUDF/XDF field (Beckwith et al. 2006; Illingworth et al. 2013; Ellis et al. 2013). Additional imaging over these fields was taken over the years by a very large number of programs. A complete listing of HST programs can be found on the Hubble Legacy Field (HLF) release page[3] (see also Whitaker et al. 2019 and Illingworth et al. 2016).

These fields are thus among the most valuable extragalactic legacy fields, especially for distant galaxy science. More than 40% of all HST-selected $z \sim 7 - 8$ candidate galaxies from blank-field surveys lie in these two areas alone (e.g. Bouwens et al. 2015a; Finkelstein et al. 2015). One of the first sources spectroscopically confirmed with Lyα at $z > 7$ lies in GOODS-N ($z = 7.5$, Finkelstein et al. 2013) within a spectroscopically confirmed overdensity of $z \sim 7.5$ galaxies (Jung et al. 2020). GOODS-N also contains the most distant confirmed galaxy with HST: GN-z11 (Oesch et al. 2016; Bunker

[1] https://github.com/gbrammer/grizli
[2] https://github.com/npirzkal/GRISMCONF
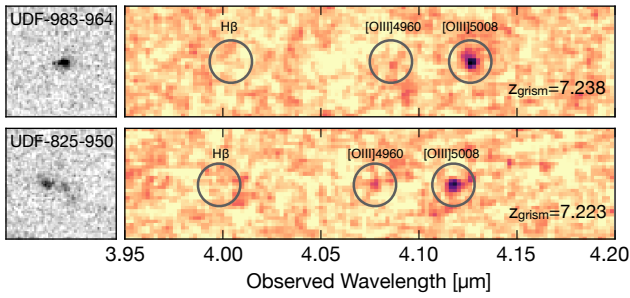
[3] https://archive.stsci.edu/prepds/hlf/

Figure 4. An example of how the NIRCam/grism data from the FRESCO survey can finally obtain spectroscopic redshift confirmation for sources that have been identified as high-redshift galaxy candidates almost 20 years prior. The two galaxies shown here have already been detected with the NICMOS camera in Bouwens et al. (2004). The left stamps correspond to the F444W direct image, while the right panels show the continuum-subtracted grism data. The [OIII] doublet is significantly detected in both cases resulting in an unambiguous redshift confirmation. The Hβ line is found to be weaker for both sources. This example demonstrates the power of NIRCam/grism observations to obtain an emission line selected census of galaxies in the epoch of reionization.

et al. 2023), a dusty, red QSO at $z \sim 7$ (Fujimoto et al. 2022), as well as an enigmatic dusty source, HDF850.1, embedded in another overdensity at $z \sim 5.2$ (Walter et al. 2012). By targeting both GOODS fields, FRESCO thus enables a first estimate of the diversity of cosmic structures across cosmis history, well into the EoR.

Both of the FRESCO fields are (partially) observed with the proprietary NIRCam/GTO data from the JADES survey (Eisenstein et al. 2023; see also Helton et al. 2023), and with two of the MIRI GTO programs (Rieke et al, in prep.; Ostlin et al, in prep.; see also Rieke et al. 2015; Rinaldi et al. 2023). Additionally, the FRESCO data overlap with the public programs JEMS (Williams et al. 2023) and NGDEEP (Bagley et al. 2023).

2.4 Data Acquisition

The FRESCO survey design results in a total science time of 35.5 hrs, for a total of 53.8 hrs including overheads. The FRESCO-S data in the GOODS-South field were acquired between Nov 13 and Nov 18, 2022, at an orientation of ∼0 deg (V3PA in the range 353.9 to 0.6). The FRESCO-N data in the GOODS-North field were obtained between Feb 11 and 13, 2023, at an orientation of 230.5 (V3PA in the range 230.37-230.59). The central position of FRESCO-N was offset slightly from the center of the CANDELS/Deep region in order to capture a few high-profile objects and an expected overdensity of $z \sim 7.5$ galaxies, as discussed in the previous section.

3 SCIENTIFIC GOALS

FRESCO exploits the unique capability of the NIRCam/grism to obtain deep spectra at ∼4-5μm for the entire survey field. This enables a wealth of both targeted science, as well as serendipitous discovery. Below, we discuss some of the most important scientific questions the community can address with these data.
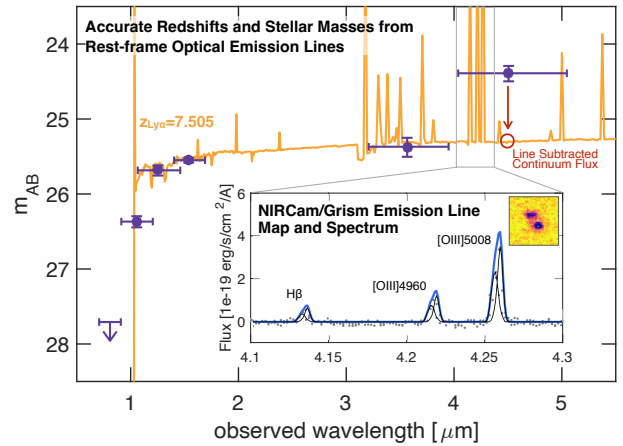
Figure 5. At $z > 5$, the rest-frame optical [OIII]+Hβ lines are found to have observed-frame EWs of > 5000 Å – on average (Labbé et al. 2010). This enables extremely efficient spectroscopic confirmation (inset). However, such strong lines contaminate broad-band photometry, as clearly seen in the IRAC CH2 photometry of this source. This can result in stellar mass uncertainties of up to $5 - 10\times$. FRESCO's spectra enable us to correct JWST's broad-band photometry to obtain true rest-frame optical continuum and hence stellar mass measurements.

3.1 Spectroscopic Census of Early Galaxy Build-up

3.1.1 Spectroscopic Redshifts in the Heart of Reionization

The first 1 Gyr of cosmic history that constitute the cosmic reionization epoch remain a key unknown in our understanding of the Universe's evolution (see recent reviews Dayal & Ferrara 2018; Robertson 2022). Despite enormous efforts, the galaxies in the EoR have eluded almost all attempts at spectroscopic characterization before JWST, apart from a handful of especially bright (or lensed) galaxies. Only two dozen "normal" galaxies had confirmed spectroscopic redshifts at $z > 7$, out of more than 2000 candidates that were known from prime extragalactic HST legacy fields alone (Fig. 2; e.g., Bouwens et al. 2015b; Finkelstein et al. 2015; Atek et al. 2018). The main reason for this difficulty was that the primary line for redshift confirmations, Lyα, is severely attenuated at $z > 6$ due to absorption in the largely neutral intergalactic medium (e.g., Dijkstra 2014; Mason et al. 2018). With JWST, this critical shortcoming can finally be overcome through rest-frame optical spectroscopy. FRESCO probes the [OIII]+Hβ emission lines of galaxies at $z = 6.7 - 9.0$ as well as Hα for sources at $z = 4.9 - 6.7$. The spectroscopically confirmed redshifts allow us to probe the small scale clustering and 3D correlation function of galaxies during the reionization epoch (e.g., Endsley et al. 2020). From simulations, the progress of reionization is expected to be correlated with the underlying density field (see Fig. 3; Qin et al. 2022; Leonova et al. 2022).

Figure 4 demonstrates the power of FRESCO's NIRCam/grism spectra to measure the redshifts of EoR galaxies. The two highlighted sources are Lyman break galaxies (LBGs) that were identified almost 20 years ago by Bouwens et al. (2004) from the HST/NICMOS images over the Hubble Ultra Deep Field (Thompson et al. 2005). With FRESCO, their high-redshift nature is confirmed through the detection of the [OIII]$\lambda\lambda$4960,5008 doublet at $z_{\mathrm{grism}} = 7.238$ and $z_{\mathrm{grism}} = 7.223$, respectively. Importantly, these objects were not selected prior to the observations: all objects in the field are observed spectroscopically, without the need to pre-select targets. This is the main advantage of grism observations and enables a very wide array of science.
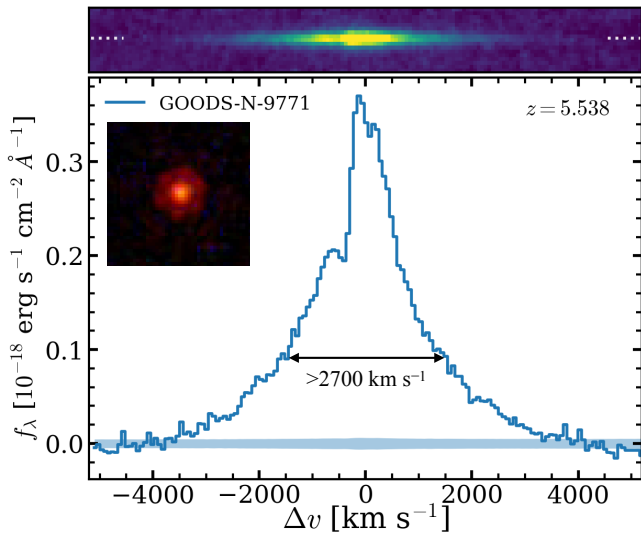
Figure 6. An example of a serendipitously discovered broad-line, low-mass AGN from FRESCO spectra. The extremely broad Hα+[NII] lines identify these galaxies as hosting massive black holes (for more information, see Matthee et al. 2023a). NIRCam/grism observations are uniquely capable of discovering such sources and confirming their number densities in the future. Given the high spectral resolution of $R \sim 1600$, such observations also have the power to reveal kinematic information for less extreme galaxies.

3.1.2 Accurate Stellar Masses in the Heart of Reionization

From HST+Spitzer observations, it has been known for several years that the emission line strengths of [OIII] or Hα are rapidly increasing toward higher redshift (e.g. Schaerer & de Barros 2010; Fumagalli et al. 2012; Labbé et al. 2013), resulting in observed-frame equivalent widths that are >5000 Å on average (e.g., Smit et al. 2014; Roberts-Borsani et al. 2016; De Barros et al. 2019; Endsley et al. 2021). This evolution has dramatic consequences for stellar mass estimates that can remain uncertain by factors up to 5-10$\times$ (Fig 5) – a problem that still applies to NIRCam imaging. Bisigello et al. 2019 estimate *median* correction factors up to 0.87dex, if strong emission lines are not accounted for. FRESCO provides emission line measurements for all sources in the field, enabling precise corrections of the broad-band fluxes for emission line contamination on a source-by-source basis. A prominent example is shown in Figure 5. The source in question still has one of the most distant Lyα detections at $z_{Ly\alpha} = 7.5$ (Finkelstein et al. 2013; Jung et al. 2020). Thanks to this, it was clear that the excess in the IRAC 4.5μm band was due to strong rest-frame optical emission lines. Nevertheless, the strength of these lines was uncertain. The FRESCO data shows that the source is actually composed of two components with slightly offset velocities. For both components, the contribution of these emission lines to the broad-band photometry can now be assessed separately. With these corrections, FRESCO thus provides accurate stellar mass measurements over two deep key fields. Additionally, it will enable the derivation of statistical correction factors for other imaging surveys.

While these strong rest-optical emission lines can complicate stellar mass estimates, they enable efficient spectroscopic confirmations. Therefore, FRESCO's spectra continue to propel the spectroscopic frontier into the heart of cosmic reionization by obtaining redshifts down to 0.2-0.5 $L*$ at $z \sim 7 - 9$ (see Fig 2). This critically enables measurements of the UV luminosity and stellar mass functions based on pure spectroscopic samples at $z \gtrsim 5$.
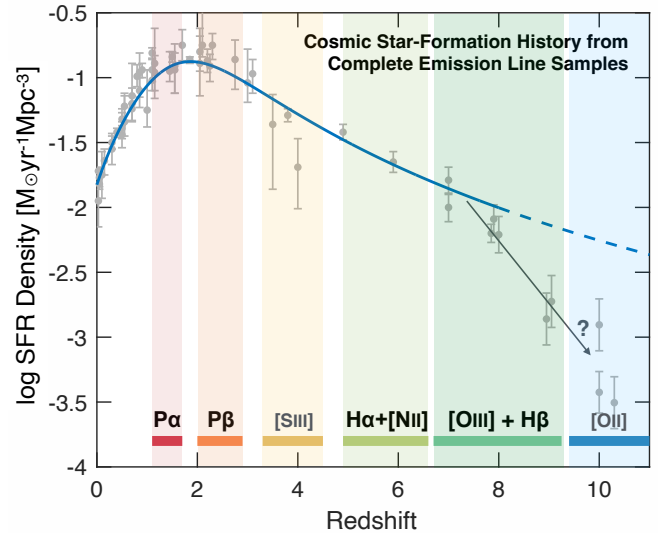
Figure 7. FRESCO is designed to return a complete sample of star-forming galaxies based on emission lines across the majority of cosmic history. FRESCO 4-5μm spectra (a) directly constrain the debated accelerated evolution of the SFRD at $z > 8$ based on [OIII]+Hβ samples at z =6.9-9.0; (b) follow galaxy build-up through the reionization epoch with Hα+[NII] measurements at z =4.9-6.6; and (c) probe the peak of cosmic SF ($z\sim$1-3) through dust-insensitive Paα and Paβ maps. In the local Universe, FRESCO even covers PAH lines at 3.3 μm for a small number of galaxies (see also Fig 8).

3.1.3 Metal-Free Star Formation and the Build-up of Metals at $z > 3$

A major question for extragalactic surveys with JWST remains whether it is possible to detect primordial (PopIII/zero-metallicity) star formation. While candidate PopIII galaxies at $z \sim 7$ have been claimed in the literature (e.g., Sobral et al. 2015), none have been confirmed (see, e.g., Bowler et al. 2017; Matthee et al. 2017). FRESCO has a unique discovery potential for extremely low metallicity candidates at $z > 6$. The medium-band imaging at 1.8-2 μm will result in improved UV continuum slope measurements at $z \sim 7 - 9$ enabling the identification of especially blue galaxies for which the grism [OIII] and Hβ line ratios provide an initial gas-phase metallicity estimate ([OIII]/Hβ decreases at $< 0.2Z_\odot$; e.g., Maiolino et al. 2008; Inoue 2011; Curti et al. 2020). FRESCO thus has the capability to provide promising, extremely metal-poor candidates for future NIRSpec follow-up. At $z \sim 4.9 - 6.6$, FRESCO continues to trace the build-up of metals through [NII]/Hα line ratios in order to constrain the mass-metallicity relations and models of early chemical enrichment. As such, FRESCO data allows us to trace the transition from extremely metal poor star formation at $z > 6$ to more enriched conditions that are found at later times.

3.1.4 The Prevalence of AGN among Early Galaxies

Another central question of extragalactic astronomy is the abundance of active galactic nuclei (AGN) in the early Universe. These sources could provide a non-negligible contribution to reionization (e.g., Madau & Haardt 2015; Giallongo et al. 2015), and are expected to explain the abundances of super-massive black holes at later times (e.g., Volonteri 2010). Interestingly, several of the most luminous $z \sim 7 - 9$ galaxies show indications for AGN activity, based on
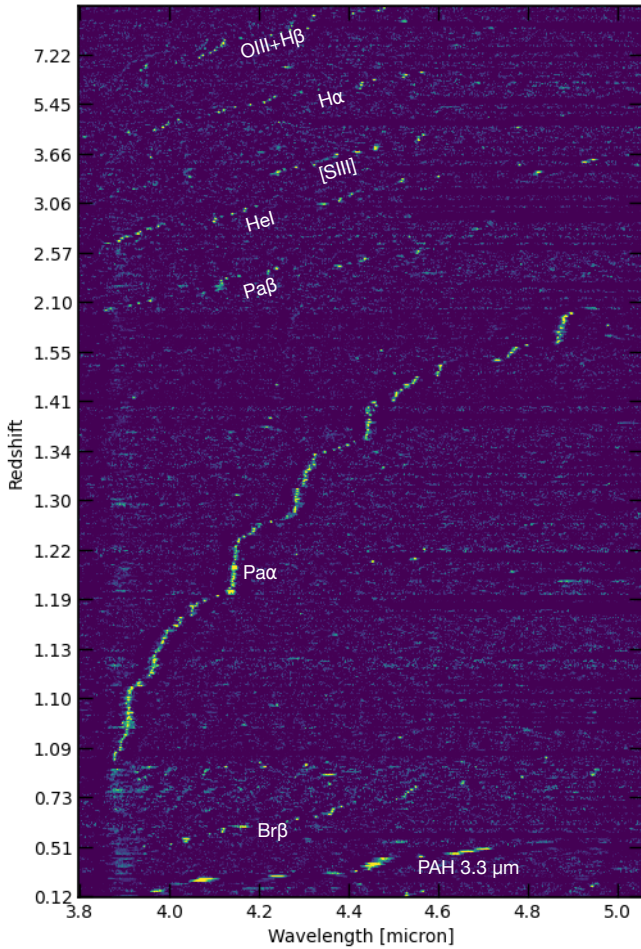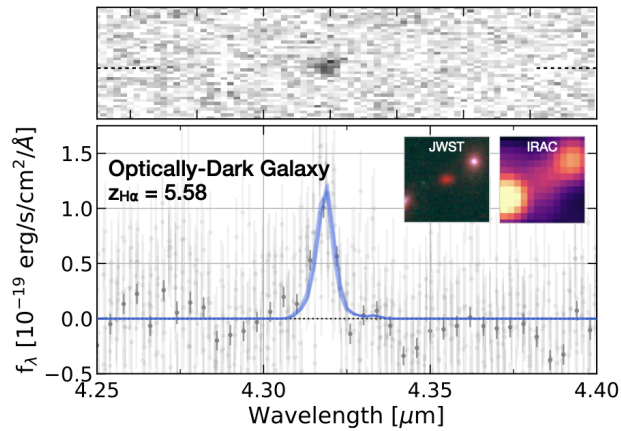
Figure 10. FRESCO's imaging and spectroscopy has the power to reveal the nature of the enigmatic population of optically-faint galaxies. Shown is an example galaxy from Xiao et al. (in prep.) in the FRESCO-S field. The source was known from ALMA, but its counterpart could not be identified in the low-spatial resolution IRAC imaging. FRESCO's F444W images clearly reveal this galaxy, and with the NIRCam/grism spectra its redshift can be determined through the Hα emission line.

instance, Hα maps from HST grism observations of $z \sim 1-2$ galaxies have been used to reveal star-forming clumps and centrally suppressed star formation in massive galaxies, consistent with inside-out growth (e.g. Wuyts et al. 2013; Nelson et al. 2016). This appears to hold, even when accounting for dust gradients inferred from resolved broadband colors or stacked Balmer decrements (e.g. Tacchella et al. 2018). However, ALMA observations of the 870μm dust continuum emission show a different picture: the dust continuum in many massive galaxies is centrally concentrated (Tadaki et al. 2020). These observations support a different scenario, in which violent dissipative events fuel nuclear star formation. Given the uncertainties in Hα dust corrections and complications in the interpretation of the dust continuum emission (e.g., due to different heating mechanisms, dust temperature gradients, insensitivity to diffuse emission), an instantaneous and dust-insensitive tracer of star formation is critically needed. FRESCO provides exactly this, with spatially resolved measurements of the Paschen series lines at $z \sim 1-3$. These measurements allow us to finally answer the question: do massive galaxies at cosmic noon form their last stars in their centers or in their outskirts before they quench?

A first example of a resolved Paα map in the FRESCO-S field is shown in Figure 9. The `grizli`-generated Paα map indeed reveals a very compact star-forming core for this galaxy that is completely absent in the shorter wavelength imaging. This is embedded in more extended star-formation throughout the galaxy. NIRCam/grism observations such as from FRESCO enable systematic studies of the spatial distribution of star-formation in cosmic noon galaxies.

3.2.3 Illuminating the Complex ISM in Assembling Galaxies

At $z > 5$, galaxies are rapidly assembling, resulting in highly complex interstellar media, as demonstrated by ALMA observations of EoR galaxies, where spatial offsets between the rest-UV continuum, and different ISM lines such as [CII] or [OIII]88μm are common (e.g., Maiolino et al. 2015; Carniani et al. 2017). FRESCO provides detailed Hα (Hβ) maps of a large sample of galaxies at $z = 4.9 - 6.6$ ($z = 6.7 - 9.0$) to constrain how and where within galaxies stars are forming during the epoch of reionization (for first examples see
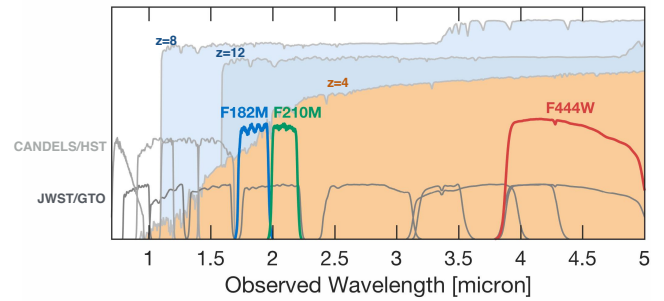

Figure 11. FRESCO obtains images in two medium-band filters at $\sim 2\mu$m (and a direct image in F444W). These data seamlessly extend HST's legacy imaging over these fields and complement the GTO data resulting in vast improvements in UV-continuum slope measurements for $z > 6$ galaxies and enabling the selection of quiescent galaxies up to $z \sim 4$.

the EIGER program Matthee et al. 2023b). Comparisons between Hα and rest-optical continuum sizes provide a first test of inside-out growth during an epoch when galaxies are still assembling – rather than fully settled in – (cold) disks, or may reveal homologous growth with a similar pace of stellar build-up across all radii.

3.2.4 Illuminating the Dark Side of Star-Formation

Over the past few years it has become more and more clear that HST-based surveys have been missing a potentially important population of massive, star-forming galaxies at $z > 3$ that are sufficiently obscured such that they remained undetected at rest-UV wavelengths (e.g., Caputi et al. 2015; Franco et al. 2018; Alcalde Pampliega et al. 2019; Wang et al. 2019; Fudamoto et al. 2021; Xiao et al. 2023). These galaxies have been identified either through Spitzer/IRAC or through ALMA observations. However, given the limited photometry available, their photometric redshifts and thus also their nature remained highly uncertain. With JWST we can now finally probe the rest-frame optical wavelengths up to $z \sim 9$, which brings this optically-faint galaxy population into view (e.g., Barrufet et al. 2023; Rodighiero et al. 2023; Pérez-González et al. 2023). FRESCO's imaging and spectroscopy is especially powerful to characterize this enigmatic population of galaxies. The grism spectra enable – for the first time – to obtain spectroscopic redshifts for such galaxies thanks to emission line searches. An example of this is shown in Fig 10 of a galaxy that has previously been detected only at sub-millimeter wavelengths (Cowie et al. 2018; Yamaguchi et al. 2019; Gómez-Guijarro et al. 2022; Xiao et al. 2023, Xiao et al. in prep).

3.2.5 The Emergence of Quiescent Galaxies

At $z < 2$, the massive galaxy population is dominated by dead, quiescent galaxies, with no significant ongoing star formation (e.g., Muzzin et al. 2013; Davidzon et al. 2017). However, it is still unknown when such quiescent galaxies first appeared in the Universe. Deep ground-based K-band surveys demonstrated that quiescent galaxies existed since $z \sim 4$, however, their exact number densities remain debated (Straatman et al. 2015; Davidzon et al. 2017; Forrest et al. 2020; Valentino et al. 2020), mainly because HST-based surveys are limited to rest-frame optical observations at $z < 2.5$. First searches with JWST are already finding and confirming quiescent, low star-formation rate galaxies up to $z \sim 5 - 7$ (see, e.g., Valentino et al. 2023; Carnall et al. 2023; Looser et al. 2023). A large population of such sources in the very early Universe challenges simulations (e.g.,

Wellons et al. 2015; Merlin et al. 2019; Hartley et al. 2023), such that the timing of when massive galaxies grow, shut off their star formation and turn quiescent is a very powerful constraint on galaxy evolution models.

The short-wavelength imaging from FRESCO is designed to complement the JADES/GTO broad-band data in these fields and seamlessly extends HST's legacy data to enable accurate selections of quiescent galaxies up to $z \sim 4$ from Balmer break measurements (see Fig. 11). In the SW channel, the imaging filters are the same as obtained with the JEMS survey over the HUDF/XDF.

3.3 Legacy Science

The CANDELS/Deep fields in the centers of GOODS-S and -N are two of the most studied areas in the sky with the most comprehensive ancillary data. FRESCO builds on these data and further increases the legacy value of these fields beyond that of the GTO teams by enabling a more complete census of emission line galaxies through blind spectroscopy. Among others, FRESCO provides emission samples for future spectroscopic follow-up with NIRSpec. Thus, FRESCO's zero-proprietary data enable a wealth of legacy science to be performed by the community. First science papers by the community using FRESCO imaging and spectroscopy have already been published as pre-prints (Laporte et al. 2022; Helton et al. 2023).

4 SUMMARY

This paper provided an overview of the medium program FRESCO – a NIRCam grism spectroscopy and imaging survey of two fields in the GOODS-North and -South fields, respectively. The power of NIRCam/grism observations are clearly demonstrated with this survey: the grism provides $R \sim 1600$ spectroscopy of all sources in the field of view in its long-wavelength channel, while imaging is obtained in a short-wavelength filter at the same time. Adopting this strategy with the F444W filter, FRESCO obtained deep spectra covering 3.8-5.0 μm, reaching average line sensitivities of $2 \times 10^{-18} \mathrm{erg\,s^{-1}\,cm^{-2}}$ (5σ). At the same time, deep F182M and F210M images are obtained reaching ~ 28.2 mag rms (5σ in $0\farcs32$ diameter apertures), together with F444W direct images reaching similar depth. The FRESCO observations thus significantly enhance the rich ancillary dataset in these key legacy fields, enabling a vast amount of science by the community. The spectral coverage allows one to probe emission line galaxies across almost the full cosmic history. We have highlighted a few science cases, that showcase the enormous power for serendipitous discovery of such NIRCam/grism observations. Future, wider-area grism programs would thus be able to obtain large, complete samples of rare classes of galaxies that will be very difficult to follow-up, e.g., with NIRSpec spectroscopy through targeted programs. We hope that the community will use the FRESCO dataset for a large number of scientific discoveries as well as as inspiration for many further JWST programs, including NIRCam/grism observations.

DATA AVAILABILITY

The HST and JWST image mosaics of the FRESCO fields are already released at MAST as a High Level Science Product via https://doi.org/10.17909/gdyc-7g80. The spectra are still being calibrated and will be made available together with an upcoming data paper (Brammer et al., in prep.). For updates, please check our webpage: https://jwst-fresco.astro.unige.ch/ or the MAST page https://archive.stsci.edu/hlsp/fresco/.

AFFILIATIONS

[1]*Department of Astronomy, University of Geneva, Chemin Pegasi 51, 1290 Versoix, Switzerland*
[2]*Cosmic Dawn Center (DAWN), Niels Bohr Institute, University of*

Copenhagen, Jagtvej 128, København N, DK-2200, Denmark

[3] *MIT Kavli Institute for Astrophysics and Space Research, 77 Massachusetts Ave., Cambridge, MA 02139, USA*

[4] *Leiden Observatory, Leiden University, NL-2300 RA Leiden, Netherlands*

[5] *Department of Astronomy, The University of Texas at Austin, 2515 Speedway, Stop C1400, Austin, TX 78712-1205, USA*

[6] *Department of Astronomy and Astrophysics, University of California, Santa Cruz, CA 95064, USA*

[7] *Department of Physics, ETH Zürich, Wolfgang-Pauli-Strasse 27, Zürich, 8093, Switzerland*

[8] *Department for Astrophysical and Planetary Science, University of Colorado, Boulder, CO 80309, USA*

[9] *School of Physics, University of Melbourne, Parkville, VIC 3010, Australia*

[10] *ARC Centre of Excellence for All Sky Astrophysics in 3 Dimensions (ASTRO 3D), Australia*

[11] *Department of Physics and Astronomy, University of California, Riverside, 900 University Avenue, Riverside, CA 92521, USA*

[12] *Department of Physics & Astronomy, University of California, Los Angeles, 430 Portola Plaza, Los Angeles, CA 90095, USA*

[13] *Steward Observatory, University of Arizona, Tucson, AZ 85721, USA*

[14] *Astronomy Department, Yale University, 52 Hillhouse Ave, New Haven, CT 06511, USA*

[15] *Department of Astronomy, University of Massachusetts, Amherst, MA 01003, USA*

[16] *Department of Physics, University of Bath, Claverton Down, Bath, BA2 7AY, UK*

[17] *Waseda Research Institute for Science and Engineering, Faculty of Science and Engineering, Waseda University, 3-4-1 Okubo, Shinjuku, Tokyo 169-8555, Japan*

[18] *National Astronomical Observatory of Japan, 2-21-1, Osawa, Mitaka, Tokyo, Japan*

[19] *Kapteyn Astronomical Institute, University of Groningen, P.O. Box 800, 9700 AV Groningen, The Netherlands*

[20] *Centre for Astrophysics and Supercomputing, Swinburne University of Technology, Melbourne, VIC 3122, Australia*

[21] *GRAPPA, Anton Pannekoek Institute for Astronomy and Institute of High-Energy Physics*

[22] *University of Amsterdam, Science Park 904, NL-1098 XH Amsterdam, the Netherlands*

[23] *Department of Physics and Astronomy, Tufts University, 574 Boston Avenue, Medford, MA 02155, USA*

[24] *Department of Astronomy, University of Wisconsin-Madison, 475 N. Charter St., Madison, WI 53706 USA*

[25] *Max Planck Institut für Astronomie, Königstuhl 17, D-69117, Heidelberg, Germany*

[26] *Astrophysics Research Institute, Liverpool John Moores University, 146 Brownlow Hill, Liverpool L3 5RF, UK*

[27] *Departament d'Astronomia i Astrofísica, Universitat de València, C. Dr. Moliner 50, E-46100 Burjassot, València, Spain*

[28] *Unidad Asociada CSIC "Grupo de Astrofísica Extragaláctica y Cosmología" (Instituto de Física de Cantabria - Universitat de València)*

REFERENCES

Adams N. J., et al., 2023, MNRAS, 518, 4755

Alcalde Pampliega B., et al., 2019, ApJ, 876, 135

Arrabal Haro P., et al., 2023, arXiv e-prints, p. arXiv:2303.15431

Astropy Collaboration et al., 2013, A&A, 558, A33

Astropy Collaboration et al., 2018, AJ, 156, 123

Atek H., et al., 2010, ApJ, 723, 104

Atek H., Richard J., Kneib J.-P., Schaerer D., 2018, MNRAS, 479, 5184

Atek H., et al., 2023, MNRAS, 519, 1201

Bagley M. B., et al., 2023, arXiv e-prints, p. arXiv:2302.05466

Bakx T. J. L. C., et al., 2020, MNRAS, 493, 4294

Barrufet L., et al., 2023, MNRAS, 522, 449

Beckwith S. V. W., et al., 2006, AJ, 132, 1729

Bertin E., Arnouts S., 1996, A&AS, 117, 393

Bisigello L., et al., 2019, ApJS, 243, 27

Bouwens R. J., Illingworth G. D., Blakeslee J. P., Broadhurst T. J., Franx M., 2004, ApJ, 611, L1

Bouwens R. J., et al., 2015a, ApJ, 803, 34

Bouwens R. J., et al., 2015b, ApJ, 803, 34

Bouwens R. J., et al., 2022, ApJ, 931, 160

Bouwens R., Illingworth G., Oesch P., Stefanon M., Naidu R., van Leeuwen I., Magee D., 2023, MNRAS, 523, 1009

Bowler R. A. A., McLure R. J., Dunlop J. S., McLeod D. J., Stanway E. R., Eldridge J. J., Jarvis M. J., 2017, MNRAS, 469, 448

Brammer G., 2018, Gbrammer/Grizli: Preliminary Release, Zenodo, doi:10.5281/zenodo.1146905

Brammer G. B., van Dokkum P. G., Coppi P., 2008, ApJ, 686, 1503

Brammer G. B., et al., 2012, ApJS, 200, 13

Brammer G., Strait V., Matharu J., Momcheva I., 2022, grizli, Zenodo, doi:10.5281/zenodo.6672538

Bunker A. J., et al., 2023, arXiv e-prints, p. arXiv:2302.07256

Caputi K. I., et al., 2015, ApJ, 810, 73

Carnall A. C., et al., 2023, MNRAS, 518, L45

Carniani S., et al., 2017, A&A, 605, A42

Casey C. M., Narayanan D., Cooray A., 2014, Phys. Rep., 541, 45

Casey C. M., et al., 2018, ApJ, 862, 77

Cleri N. J., et al., 2022, ApJ, 929, 3

Cowie L. L., González-López J., Barger A. J., Bauer F. E., Hsu L. Y., Wang W. H., 2018, ApJ, 865, 106

Curti M., Mannucci F., Cresci G., Maiolino R., 2020, MNRAS, 491, 944

Curtis-Lake E., et al., 2022, arXiv e-prints, p. arXiv:2212.04568

Davidzon I., et al., 2017, A&A, 605, A70

Dayal P., Ferrara A., 2018, Phys. Rep., 780, 1

De Barros S., Oesch P. A., Labbé I., Stefanon M., González V., Smit R., Bouwens R. J., Illingworth G. D., 2019, MNRAS, 489, 2355

Dijkstra M., 2014, Publ. Astron. Soc. Australia, 31, e040

Donnan C. T., et al., 2023, MNRAS, 518, 6011

Eisenstein D. J., et al., 2023, arXiv e-prints, p. arXiv:2306.02465

Ellis R. S., et al., 2013, ApJ, 763, L7

Endsley R., Behroozi P., Stark D. P., Williams C. C., Robertson B. E., Rieke M., Gottlöber S., Yepes G., 2020, MNRAS, 493, 1178

Endsley R., Stark D. P., Chevallard J., Charlot S., 2021, MNRAS, 500, 5229

Endsley R., Stark D. P., Whitler L., Topping M. W., Chen Z., Plat A., Chisholm J., Charlot S., 2023, MNRAS, 524, 2312

Estrada-Carpenter V., et al., 2019, ApJ, 870, 133

Fanelli M. N., O'Connell R. W., Thuan T. X., 1988, ApJ, 334, 665

Finkelstein S. L., 2016, Publ. Astron. Soc. Australia, 33, e037

Finkelstein K. D., et al., 2011, ApJ, 742, 108

Finkelstein S. L., et al., 2013, Nature, 502, 524

Finkelstein S. L., et al., 2015, ApJ, 810, 71

Finkelstein S. L., et al., 2022, ApJ, 928, 52

Forrest B., et al., 2020, ApJ, 903, 47

Franco M., et al., 2018, A&A, 620, A152

Fudamoto Y., et al., 2021, Nature, 597, 489

Fujimoto S., et al., 2022, Nature, 604, 261

Fumagalli M., et al., 2012, ApJ, 757, L22

Furtak L. J., Atek H., Lehnert M. D., Chevallard J., Charlot S., 2021, MNRAS, 501, 1568

Genzel R., Cesarsky C. J., 2000, ARA&A, 38, 761

Giallongo E., et al., 2015, A&A, 578, A83

Giavalisco M., Steidel C. C., Macchetto F. D., 1996, ApJ, 470, 189

Gómez-Guijarro C., et al., 2022, A&A, 658, A43
Grogin N. A., et al., 2011, ApJS, 197, 35
Harikane Y., et al., 2022, ApJ, 929, 1
Harikane Y., et al., 2023, arXiv e-prints, p. arXiv:2303.11946
Hartley A. I., et al., 2023, MNRAS, 522, 3138
Hashimoto T., et al., 2018, Nature, 557, 392
Helton J. M., et al., 2023, arXiv e-prints, p. arXiv:2302.10217
Hunter J. D., 2007, Computing In Science & Engineering, 9, 90
Illingworth G. D., et al., 2013, ApJS, 209, 6
Illingworth G., et al., 2016, arXiv e-prints, p. arXiv:1606.00841
Inami H., et al., 2017, A&A, 608, A2
Inoue A. K., 2011, MNRAS, 415, 2920
Inoue A. K., et al., 2016, Science, 352, 1559
Juneau S., Dickinson M., Alexander D. M., Salim S., 2011, ApJ, 736, 104
Jung I., et al., 2020, ApJ, 904, 144
Kashino D., Lilly S. J., Matthee J., Eilers A.-C., Mackenzie R., Bordoloi R., Simcoe R. A., 2023, ApJ, 950, 66
Kennicutt R. C., Evans N. J., 2012, ARA&A, 50, 531
Kim J. H., et al., 2012, ApJ, 760, 120
Kluyver T., et al., 2016, in Loizides F., Schmidt B., eds, Positioning and Power in Academic Publishing: Players, Agents and Agendas. pp 87 – 90
Kocevski D. D., et al., 2023, arXiv e-prints, p. arXiv:2302.00012
Koekemoer A. M., et al., 2011, ApJS, 197, 36
Labbé I., et al., 2010, ApJ, 708, L26
Labbé I., et al., 2013, ApJ, 777, L19
Labbe I., et al., 2023, arXiv e-prints, p. arXiv:2306.07320
Laporte N., Nakajima K., Ellis R. S., Zitrin A., Stark D. P., Mainali R., Roberts-Borsani G. W., 2017, ApJ, 851, 40
Laporte N., Ellis R. S., Witten C. E. C., Roberts-Borsani G., 2022, arXiv e-prints, p. arXiv:2212.05072
Le Fèvre O., et al., 2015, A&A, 576, A79
Leonova E., et al., 2022, MNRAS, 515, 5790
Looser T. J., et al., 2023, arXiv e-prints, p. arXiv:2302.14155
Madau P., Dickinson M., 2014, ARA&A, 52, 415
Madau P., Haardt F., 2015, ApJ, 813, L8
Maiolino R., et al., 2008, A&A, 488, 463
Maiolino R., et al., 2015, MNRAS, 452, 54
Mason C. A., Treu T., Dijkstra M., Mesinger A., Trenti M., Pentericci L., de Barros S., Vanzella E., 2018, ApJ, 856, 2
Matthee J., et al., 2017, ApJ, 851, 145
Matthee J., et al., 2023a, arXiv e-prints, p. arXiv:2306.05448
Matthee J., Mackenzie R., Simcoe R. A., Kashino D., Lilly S. J., Bordoloi R., Eilers A.-C., 2023b, ApJ, 950, 67
Merlin E., et al., 2019, MNRAS, 490, 3309
Momcheva I. G., et al., 2016, ApJS, 225, 27
Muzzin A., et al., 2013, ApJ, 777, 18
Naidu R. P., et al., 2022, ApJ, 940, L14
Nelson E. J., et al., 2016, ApJ, 828, 27
Nelson E. J., et al., 2023, ApJ, 948, L18
Oesch P. A., et al., 2015, ApJ, 804, L30
Oesch P. A., et al., 2016, ApJ, 819, 129
Oesch P. A., Bouwens R. J., Illingworth G. D., Labbé I., Stefanon M., 2018, ApJ, 855, 105
Oliphant T. E., 2015, Guide to NumPy. Continuum Press
Pentericci L., et al., 2014, ApJ, 793, 113
Pérez F., Granger B. E., 2007, Computing in Science and Engineering, 9, 21
Pérez-González P. G., et al., 2023, ApJ, 946, L16
Pirzkal N., et al., 2004, ApJS, 154, 501
Pirzkal N., et al., 2018, ApJ, 868, 61
Qin Y., Wyithe J. S. B., Oesch P. A., Illingworth G. D., Leonova E., Mutch S. J., Naidu R. P., 2022, MNRAS, 510, 3858
Reddy N. A., et al., 2015, ApJ, 806, 259
Reddy N. A., Topping M. W., Sanders R. L., Shapley A. E., Brammer G., 2023, ApJ, 948, 83
Rieke M. J., Kelly D., Horner S., 2005, in Heaney J. B., Burriesci L. G., eds, Society of Photo-Optical Instrumentation Engineers (SPIE) Conference Series Vol. 5904, Cryogenic Optical Systems and Instruments XI. pp 1–8, doi:10.1117/12.615554

Rieke G. H., et al., 2015, PASP, 127, 665
Rieke M. J., et al., 2023, PASP, 135, 028001
Rinaldi P., et al., 2023, ApJ, 952, 143
Roberts-Borsani G. W., et al., 2016, ApJ, 823, 143
Robertson B. E., 2022, ARA&A, 60, 121
Rodighiero G., Bisigello L., Iani E., Marasco A., Grazian A., Sinigaglia F., Cassata P., Gruppioni C., 2023, MNRAS, 518, L19
Schaerer D., de Barros S., 2009, A&A, 502, 423
Schaerer D., de Barros S., 2010, A&A, 515, A73
Schouws S., et al., 2022, arXiv e-prints, p. arXiv:2202.04080
Shivaei I., et al., 2018, ApJ, 855, 42
Smit R., et al., 2014, ApJ, 784, 58
Sobral D., Matthee J., Darvish B., Schaerer D., Mobasher B., Röttgering H. J. A., Santos S., Hemmati S., 2015, ApJ, 808, 139
Sobral D., Santos S., Matthee J., Paulino-Afonso A., Ribeiro B., Calhau J., Khostovan A. A., 2018, MNRAS, 476, 4725
Song M., et al., 2016, ApJ, 825, 5
Stark D. P., 2016, ARA&A, 54, 761
Stark D. P., Ellis R. S., Chiu K., Ouchi M., Bunker A., 2010, MNRAS, 408, 1628
Stark D. P., Schenker M. A., Ellis R., Robertson B., McLure R., Dunlop J., 2013, ApJ, 763, 129
Stark D. P., et al., 2017, MNRAS, 464, 469
Stefanon M., Bouwens R. J., Labbé I., Illingworth G. D., Gonzalez V., Oesch P. A., 2021, ApJ, 922, 29
Stefanon M., Bouwens R. J., Illingworth G. D., Labbé I., Oesch P. A., Gonzalez V., 2022, ApJ, 935, 94
Straatman C. M. S., et al., 2015, ApJ, 808, L29
Sun F., et al., 2022, arXiv e-prints, p. arXiv:2209.03374
Tacchella S., Bose S., Conroy C., Eisenstein D. J., Johnson B. D., 2018, ApJ, 868, 92
Tadaki K.-i., et al., 2020, ApJ, 901, 74
Thompson R. I., et al., 2005, AJ, 130, 1
Treu T., Schmidt K. B., Trenti M., Bradley L. D., Stiavelli M., 2013, ApJ, 775, L29
Treu T., et al., 2015, ApJ, 812, 114
Trump J. R., Hsu A. D., Fang J. J., Faber S. M., Koo D. C., Kocevski D. D., 2013, ApJ, 763, 133
Übler H., et al., 2023, arXiv e-prints, p. arXiv:2302.06647
Valentino F., et al., 2020, ApJ, 889, 93
Valentino F., et al., 2023, ApJ, 947, 20
Virtanen P., et al., 2020, Nature Methods, 17, 261
Volonteri M., 2010, A&ARv, 18, 279
Walter F., et al., 2012, Nature, 486, 233
Wang T., et al., 2019, Nature, 572, 211
Wellons S., et al., 2015, MNRAS, 449, 361
Whitaker K. E., et al., 2019, ApJS, 244, 16
Williams C. C., et al., 2023, arXiv e-prints, p. arXiv:2301.09780
Wuyts S., et al., 2013, ApJ, 779, 135
Xiao M. Y., et al., 2023, A&A, 672, A18
Yamaguchi Y., et al., 2019, ApJ, 878, 73

APPENDIX A: INFORMATION OF EXAMPLE GALAXIES

In Table A1, we provide more details for the sources that are shown in the main text.

Table A1. Source information for the example galaxies shown in Figures 4, 5, 6, 9, 10

Fig	RA	Dec	z_{grism}
4a	03:32:38.81	-27:47:07.4	7.237±0.001
4b	03:32:39.53	-27:47:17.7	7.223±0.001
5a	12:36:37.92	62:18:08.7	7.507±0.001
5b	12:36:37.87	62:18:08.5	7.498±0.001
6	12:37:07.44	62:14:50.3	5.538±0.001
9	03:32:34.04	-27:50:29.1	1.3820±0.0002
10	03:32:28.91	-27:44:31.5	5.579±0.001